MODAL ABUNDANCES, CHEMISTRY, AND SIZES OF CLASTS IN THE SEMARKONA (LL3.0) CHONDRITE BY X-RAY MAP ANALYSIS. A. Lobo[1], S. W. Wallace[2], D. S. Ebel[1,2]. [1]Department of Earth and Environmental Sciences, Lamont Doherty Earth Observatory of Columbia University, Palisades, NY, 10964-8000 (ad2922@columbia.edu), [2]Department of Earth and Planetary Sciences, American Museum of Natural History, New York, NY, 10024 (swallace@amnh.org, debel@amnh.org)

Introduction: The ordinary chondrites are the most abundant meteorites in the current and historically known record. They represent planetesimals that probably have affinities to the accreting bodies that formed the emerging planets of our solar system. Quantitative measurements of the size, abundance, distribution, and chemical compositions of the components that are combined in OC must be the basis for any deeper understanding of how these components formed and accreted into protoplanetary bodies.

Although previous studies have provided some of the requisite measurements [e.g., 1, 2], new tools make it possible to count larger areas and to obtain detailed chemical composition information at each pixel.

Methods: For this study, a polished thin section of Semarkona LL3.0 (AMNH #4128-5) was mapped with the Cameca SX100 electron microprobe at the AMNH at 15kV, 20nA current, and 15ms dwell time. X-ray intensity maps at a resolution of 10μm/pixel, were stitched together to produce elemental maps for Al, Ca, Fe, K, Mg, Na, Ni, S, Si and Ti, and red-green-blue (RGB) composite maps (e.g., Mg-Ca-Al, Si-Ca-Fe) for the whole thin section. Maps were stacked (registered) into a hyperspectral data volume for identification of inclusion boundaries. Inclusions were outlined (segmented) by hand using Adobe Illustrator and a Wacom Cintiq tablet. Analyzed area was 1567124 pixels (~157 mm^2). Figure 1 shows a portion of the complete Mg-Ca-Al map illustrating how inclusions were outlined. Mg and Si intensities in chondrules served as visual signals for estimating pyroxene and olivine ratios, and typing chondrules using the criteria of [1]. Pixel-by-pixel analysis to automate typing of chondrules has not been implemented. This division served as a basis for the pixel-by-pixel composition analysis. Small isolated olivine and metal/sulfide grains were not outlined, but instead counted with matrix. Objects too small to see clearly or without a clear contour were considered part of the matrix.

ImageJ software [3, 4] and custom IDL code were used to measure the total area of inclusions of each type, and of matrix. Modal abundances based on surface area of inclusions have been shown to be equivalent to volume fractions [5, 6]. Software tools were used to analyze, pixel-by-pixel, the composition of each inclusion and of the matrix. Here, we report results in x-ray counts, with the assumption that background corrections will be similar across all pixels. We also recover apparent (2D) chondrule size information, which can be corrected to 3D [7, 8].

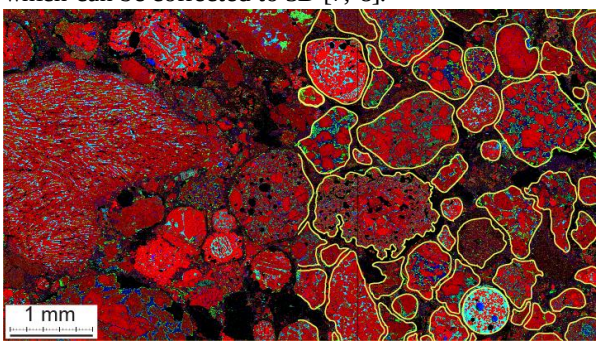

Fig. 1: Partially outlined (yellow lines, right side) region of Semarkona, in red-green-blue = Mg-Ca-Al composite. Al-rich chondrule is at lower right.

Results: Table 1 records the total area (vol%) that is accounted for by each chondrule primary textural type among all chondrules. In comparing with previous work, "granular olivine-pyroxene" and "cryptocrystalline" of [1, their Table 3] and [2] have been grouped with porphyritic olivine-pyroxene and radiating pyroxene, respectively. In this work, one Al-rich chondrule was found (Fig. 1). Type "unclassified" reports chondrules of ambiguous type.

Table 1: Previously reported chondrule type abundances, and present results, as percentage of area.

	[1]	[2]	this work
barred olivine BO	4	4	2.0
porphyritic olivine PO	27	23	23.4
porph. olivine-pyroxene POP	49	51	32.5
porph. pyroxene PP	9	10	24.3
radiating pyroxene RP	11	12	12.6
unclassified			5.0
Al-rich chondrule			0.2
No. chondrules (*n*)	545		432

The data collected here allows an analytical focus on element distributions between inclusions and matrix, relative to bulk composition. Table 2 documents the distribution of elements (as x-ray counts) across all pixels between inclusions and matrix.

Table 2: Fractions of total x-ray intensity (counts) for major elements, and fraction of total pixels (area), accounted for by all inclusions, and by matrix.

	Si	Mg	Al	Ca	Ti	Fe	S	Ni	Na	area
incIns	0.81	0.86	0.80	0.81	0.76	0.59	0.51	0.35	0.78	0.73
matrix	0.19	0.14	0.20	0.19	0.24	0.41	0.49	0.65	0.22	0.27

Table 2 also reports the total area accounted for by matrix, 27%. This is higher than previously published values, e.g., 15.6% [9]. From image analysis of 60

mm^2 of Semarkona, [10] report 76.9% vol% chondrules, with the remainder matrix, metal and FeS (here all included as matrix), similar to our result.

Table 3 reports the distribution of elements relative to Si among various components. Values for counts directly correlate to numbers of atoms.

Table 3: Ratios of total counts over total Si counts.

	Ti/Si	Mg/Si	Al/Si	Fe/Si	Ca/Si	S/Si	Ni/Si	Na/Si	n
Mg-rich chondrules	0.016	1.072	0.099	0.119	0.041	0.085	0.006	0.098	431
Al-rich chondrule	0.047	1.202	0.485	0.064	0.225	0.063	0.008	0.096	1
All chondrules	0.014	1.072	0.086	0.103	0.036	0.085	0.006	0.098	432
Matrix	0.021	0.731	0.107	0.351	0.043	0.343	0.049	0.119	-
BULK	0.017	1.007	0.101	0.163	0.042	0.134	0.014	0.102	-

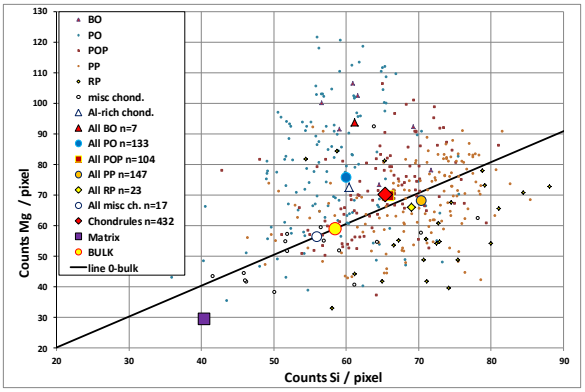

Fig. 2: Mg and Si compositions (counts/pixel) of individual clasts, and mean values for clasts, matrix, and bulk sample.

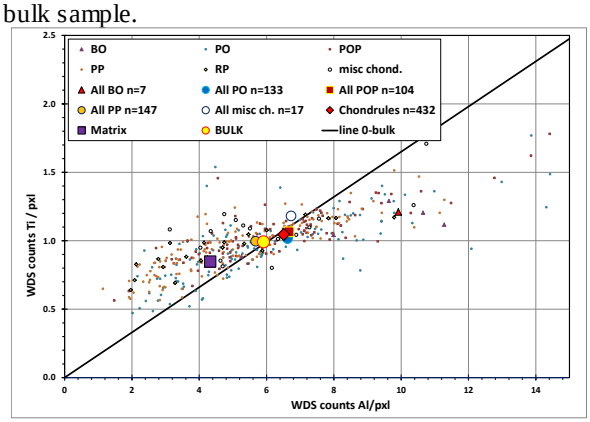

Fig. 3: Ti and Al compositions, symbols as in Fig. 2.

Values for each chondrule and the sums (total chondrule and matrix) are plotted for comparison with the bulk chemistry in Figs. 2 and 3. Matrix composition has an Mg/Si ratio below that of the bulk, with chondrule Mg/Si above bulk. The same relationship is observed in Colony (CO3.0), Kainsaz (CO3.2) [11], and Renazzo (CR2) [12].

In Fig. 3, matrix is observed to have a higher Ti/Al ratio than bulk, and chondrules slightly less than bulk. Interestingly, BO chondrules (and the Al-rich chondrule) plot well below the line connecting bulk composition to zero. It is possible that small inclusions below our detection limits (10 µm/pixel), counted here as matrix, contain higher Ti contents than the chondrules. No such inclusions are observed in higher resolution x-ray mapping of Semarkona. Relative background differences for Ti and Al would simply shift axis values, but would not affect the slope of the bulk Ti/Al line (black) in Fig. 3.

From Tables 2 and 3, matrix clearly has a much higher Fe/Si and Fe/Mg ratio relative to the bulk. As expected, Fe is strongly unequilibrated, with a high concentration in the matrix. For Ca/Al, matrix, mean chondrules, and mean BO, PO, POP and PP all fall on a line joining bulk Ca/Al and the origin.

Mean diameter of equivalent area circles for all inclusions (D) averages 0.495mm ± 0.301 (1σ) with skewness of 1.84. On the phi scale of sedimentology, mean size is phi = 1.250 ± 0.830 (1σ). Fig. 4 illustrates histograms of uncorrected [7] apparent clast sizes, and a comparison with similar data for Renazzo (CR2), with mean D = 0.616mm ± 0.511 (1σ), phi = 1.254 ± 1.373 (1σ) and skewness 1.37 [12].

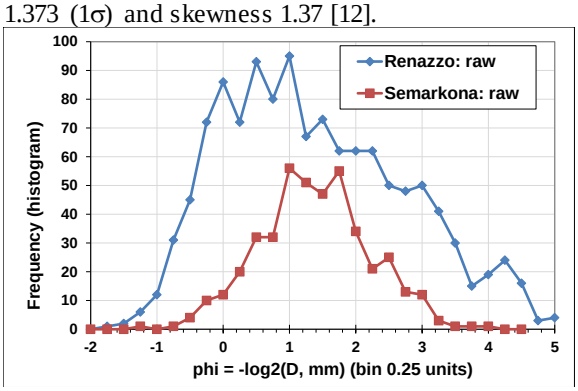

Fig. 4: Apparent (2D) size distributions of inclusions in Semarkona, and comparison to similar data for Renazzo (CR2) [12].

Discussion: The deviations from bulk composition observed in the matrix and inclusions are of opposite nature for all elements pairs except Ca and Al. This is true despite the very large spread among inclusion compositions. These ratios provide strong support for the complementarity of chondrules and matrix, as described by [13] for carbonaceous chondrites.

References: [1] Gooding J. L. and Keil K. (1981) *Meteoritics, 16*, 17-43. [2] Rubin A. E. (2000) *Earth Science Rev., 50*, 3-27. [3] Abramoff M. D et al. (2004) *Biophotonics International, 11*, 36-42. [4] http://rsb.info.nih.gov/ij/index.html [5] Chayes F. (1956) *Petrographic Modal Analysis*, Wiley (113p). [6] Dodd R. T. (1976) *Earth Planet. Sci. Letters, 30*, 281-291. [7] Eisenhour D. D. (1996) *Meteoritics Planet. Sci., 31*, 243-248. [8] Konrad K., McKnight S. V. & Ebel D. S. (2010) *LPS XLI*, Abstract #1447. [9] Huss, G. R. (1980) *Geochim. Cosmochim. Acta, 45*, 33-51. [10] Grossman J. N. and Brearley A. J. (2005) *Meteoritics Planet. Sci., 40*, 87-122. [11] Ebel D. S. et al. (2014) *LPS XLV*, Abs. #1206. [12] Bayron J. M. et al (2014) *LPS XLV*, Abs #1225. [13] Hezel D. C. and Palme H. (2010) *Earth Planet. Sci. Lett., 294*, 85-93.